LANGMUIR

Interface Components: Nanoparticles, Colloids, Emulsions, Surfactants, Proteins, Polymers

Growth of Au-Pd2Sn Nanorods via Galvanic Replacement and their Catalytic Performance on Hydrogenation and Sonogashira Coupling Reactions

Raquel Nafria, Zhishan Luo, Maria Ibáñez, Sara Martí-Sànchez, Xiaoting Yu, María de la Mata, Jordi Llorca, Jordi Arbiol, Maksym V. Kovalenko, Arnald Grabulosa, Guillermo Muller, and Andreu Cabot

Langmuir, **Just Accepted Manuscript** • DOI: 10.1021/acs.langmuir.8b02023 • Publication Date (Web): 10 Aug 2018

Growth of Au-Pd_2Sn Nanorods via Galvanic Replacement and their Catalytic Performance on Hydrogenation and Sonogashira Coupling Reactions

Raquel Nafria†,‡, Zhishan Luo†,‡, Maria Ibáñez§,⊥, Sara Martí-Sànchez∥, Xiaoting Yu†, Maria de la Mata∥, Jordi Llorca#, Jordi Arbiol∥,∇, Maksym V. Kovalenko§,⊥, Arnald Grabulosa,■ Guillermo Muller■, and Andreu Cabot*†,∇*

† Catalonia Institute for Energy Research (IREC), 08930 Sant Adrià de Besòs, Barcelona, Spain

§ Institute of Inorganic Chemistry, Department of Chemistry and Applied Biosciences, ETH Zürich, CH-8093, Switzerland

⊥ Empa-Swiss Federal Laboratories for Materials Science and Technology, Dübendorf, CH-8600, Switzerland

∥ Catalan Institute of Nanoscience and Nanotechnology (ICN2), CSIC and the Barcelona Institute of Science and Technology (BIST), Campus UAB, Bellaterra, 08193 Barcelona, Spain

Institut de Tècniques Energètiques, Universitat Politècnica de Catalunya, 08028 Barcelona, Spain

∇ ICREA, Pg. Lluís Companys 23, 08010 Barcelona, Spain

■ Departament de Química Inorgànica i Orgànica, Secció de Química Inorgànica, Universitat de Barcelona, Martí i Franquès 1-11, 08028 Barcelona, Spain

ABSTRACT

Colloidal Pd_2Sn and Au-Pd_2Sn nanorods (NRs) with tuned size were produced by the reduction of Pd and Sn salts in the presence of size- and shape-controlling agents and the posterior growth of Au tips through a galvanic replacement reaction. Pd_2Sn and Au-Pd_2Sn NRs exhibited high catalytic activity toward quasi-homogeneous hydrogenation of alkenes (styrene and 1-octene) and alkynes (phenylacetylene and 1-octyne) in dichloromethane (DCM). Au-Pd_2Sn NRs showed higher activity than Pd_2Sn for 1-octene, 1-octyne and phenylacetylene. In Au-Pd_2Sn heterostructures, XPS evidenced an electron donation from the Pd_2Sn NR to the Au tips. Such heterostructures showed distinct catalytic behaviour in the hydrogenation of compounds containing a triple bond such as tolan. This can be explained by the aurophilicity of triple bonds. To further study this effect, Pd_2Sn and Au-Pd_2Sn NRs were also tested in the Sonogashira coupling reaction between iodobenzene and phenylacetylene in DMF. At low concentration, this reaction provided the expected product, tolan. However, at high concentration, more reduced products such as stilbene and 1,2-diphenylethane were also obtained, even without the addition of H_2. A mechanism for this unexpected reduction is proposed.

INTRODUCTION

Multimetallic catalysts have associated several potential advantages over elemental compositions, including:[1–4] i) Cost reduction associated with the utilization of lower amounts of noble metals; ii) Additional degrees of freedom to tune the electronic structure toward the

creation of suitable adsorption/reaction sites; iii) Close location of different adsorption/reaction sites enabling tandem reactions that potentially reduce the number of synthetic steps toward a specific product; iv) Allow for alternative multisite reaction paths that may be faster, more selective and/or prevent poisoning species to be formed or to remain at the catalyst surface.

Multimetallic catalysts can be realized by several methods including the incorporation of multiple metallic centers within a molecule or the impregnation of the different metals on a high surface area support. However, a particularly interesting and at the same time underexploited class of catalysts is that of size-, shape- and compositional-engineered multimetallic colloidal nanoparticles (NPs). Being unsupported, essentially solution-dispersed, colloidal NPs combine the advantages of classic homogeneous and heterogeneous catalysts:[5–12] Like catalytic organic molecules, colloidal NPs can be produced with extraordinary control over chemical and structural parameters, potentially enabling the rational engineering of their catalytic activity and especially selectivity in sensitive reactions.[12–16] Colloidal NPs also have extremely high surface-to-volume ratios, which makes them potentially very active. Additionally, unlike molecular catalysts, NPs are easily separated from solvent, reactants and products, preventing product contamination and allowing catalyst reutilization in multiple cycles.

Multimetallic colloidal NPs are typically prepared by the co-reduction or thermal decomposition of precursors of the different metals and/or the heteronucleation of a second or third compound at the surface of a pre-formed NP. Additionally, atomic substitution reactions can be used to partially or totally modify the stoichiometry of pre-formed NPs obtaining new and eventually much more complex compositions. In this direction, galvanic replacement reactions, involving the substitution of lattice atoms by ions in solution mediating a redox reaction, are particularly suitable.[17–22] The galvanic replacement is driven by a difference in reduction potential between

the replacing and replaced elements, which allows the reaction to proceed at moderate temperatures and minimizing homonucleation of independent NPs. However, in spite of its high potential and versatility, very few examples exist on the modification of the composition of multimetallic nanostructures by a galvanic replacement reaction.[23,24]

The development of catalysts for organic reactions is driven by the search for cost-effective and environmentally-friendly processes suitable for a sustainable society. From the myriad of currently exploited catalytic reactions, hydrogenation and cross-coupling are among the most heavily studied. Hydrogenation comprises an exceedingly important group of reactions, including the Haber-Bosch process as well as the reduction of alkenes, aldehydes, ketones and imines.[25] On the other hand, cross-coupling reactions comprise several essential mechanistically-related reactions, including Suzuki, Stille, Heck and Sonogashira couplings among others.[26] While numerous homo- and heterogeneous catalysts have been successfully applied in these reactions, several performance, economic and impact parameters, such as activity, selectivity, substrate scope, durability/recyclability, cost-effectiveness, environmental friendliness and sustainability require further improvement, making the design of better hydrogenation and cross-coupling catalysts a worth endeavor.

Pd-based multimetallic catalysts and particularly Pd-Sn alloys have raised especial attention in these reactions owing to their reduced cost and improved performance compared to bare Pt or Pd catalysts.[16,26–31] We recently described the synthesis of Pd_2Sn nanorods (NRs) with narrow size distribution and geometry control.[16] In the present paper we report a procedure based on a galvanic replacement reaction for the growth of Au tips onto Pd_2Sn NRs to produce Au-Pd_2Sn heterostructured NRs. With both types of NRs in hand, we compare the performance of Pd_2Sn and Au-Pd_2Sn NPs in alkene and alkyne hydrogenations and in Sonogashira couplings. These

reactions have been chosen because Pd-Sn systems have been previously shown excellent performances[28] and there is also literature precedents demonstrating that supported Au NPs are active both in hydrogenation[32] and Sonogashira[33–38] couplings due the aurophilicity of alkynes.[39–41]

EXPERIMENTAL SECTION

Chemicals: Palladium(II) acetylacetonate ([$Pd(acac)_2$], 99%), tin(II) acetate ($Sn(OAc)_2$), gold(III) chloride ($AuCl_3$, 99,99%), 1-octadecene (ODE, 90%), methylamine hydrochloride (MAHC), oleylamine (OAm, >70%), hydrochloric acid (37% in water), styrene, 1-octene, phenylacetylene (PhA), 1-octyne, tolan, iodobenzene (PhI), potassium carbonate and potassium hydroxide were purchased from Sigma Aldrich. Tri-*n*-octylphosphine (TOP, 97%) was acquired from Strem. Analytical grade hexane, chloroform, *N,N*-dimethylformamide (DMF), dichloromethane, toluene and ethanol were obtained from various sources. All chemicals were used as received, except OAm, which was purified by distillation.

Synthesis of Pd_2Sn NRs: Pd_2Sn NRs were produced following our previous report[16] with a slight modification to improve the product yield while simultaneously using an air stable reactant, $Sn(OAc)_2$, instead of the air sensitive tin(II) acetylacetonate used previously. In a typical synthesis, 20 mL of OAm, 0.8 mmol of MAH, 0.3 mmol of [$Pd(acac)_2$] and 0.15 mmol $Sn(OAc)_2$ were placed in a 100 mL four-neck flask and purged under argon flow for 30 minutes at 60 °C. Then 1 mL of TOP was injected into the solution and the mixture was heated to 200 °C at 12 °C/min. After maintaining the reaction mixture at 200 °C for 30 min, the solution was heated to 300 °C at 2.5 °C/min and kept for additional 30 min at this temperature. Finally, the solution was cooled down and Pd_2Sn NRs were separated from the reaction mixture by adding

20 mL of ethanol and centrifuging at 3000 rpm for 5 min. NRs were washed with chloroform as solvent and ethanol as non-solvent by two precipitation/ redispersion steps. With the adjustment of MAHC amount, different sizes and aspect ratios of Pd_2Sn NRs were obtained, following our previous report:[16–22,] 26 ± 2 nm × 9 ± 1 nm (0.85 mmol MAHC) and 40 ± 5 nm × 11 ± 2 nm (0.9 mmol MAHC).

Synthesis of Au-Pd_2Sn NRs: Au-Pd_2Sn NRs were prepared by growing Au over Pd_2Sn NRs produced following the procedure described above. Initially, a fresh stock solution prepared in glovebox containing 0.02 mmol of $AuCl_3$ in 50 µl of OAm and 2 ml of ODE. Then, this Au stock solution was injected at room temperature into 5 mL of Pd_2Sn NRs dispersed in toluene (5 mg/mL) under strong stirring, and maintained in these conditions for 60 min. Finally, Au- Pd_2Sn NRs were washed by multiple precipitation/redispersion using toluene and ethanol. When different amounts of Au stock solution were used, different Au contents were obtained in the Pd_2Sn NRs. For too high amounts, >0.04 mmol, significant amounts of Au homogeneously nucleated in the solution.

Procedures for the catalytic runs: A) Hydrogenation reactions. An exactly weighted quantity of 10 nm Pd_2Sn or 12 nm Au-Pd_2Sn NRs (usually 10.0 mg) and the allotted quantity of substrate (styrene, 1-octene, PhA, 1-octyne or tolan) were dissolved in 20 mL of the solvent of choice under nitrogen atmosphere, sonicated for 10 minutes and transferred by syringe to a Fischer-Porter flask, which was then purged with H_2 three times, pressurised to the desired H_2 pressure (usually 3 bar) and left stirring for the selected time.

B) Sonogashira coupling reactions. An exactly weighted quantity of 10 nm Pd_2Sn or 12 nm Au-Pd_2Sn NRs (usually 10.0 mg), PhI (204 mg, 1.0 mmol), PhA (153 mg, 1.5 mmol) and base (2 mmol) were dissolved in 10 mL of dry DMF under nitrogen atmosphere, sonicated for 10

minutes and transferred by syringe to a microwave tube. The reaction was heated 130 °C for the allotted time.

The conversions in Sonogashira coupling reactions were calculated with respect to the limiting agent (PhI). The turnover frequencies (TOF) were calculated from the amount of product produced in a specific time interval in hours by considering the total Pd amount according to:

$$TOF = (mol\ product)/(mol\ Pd \cdot t)$$

Gas chromatography (GC) analyses after catalytic runs were performed with an Agilent Technologies 6890N chromatograph equipped with a HP5-5MS capillary column (30 m x 0.32 mm size) and a FID detector, with He as a carrier gas. Additionally some compounds were characterized by GC-MS analyses in an Agilent Technologies chromatograph 7820A with a mass detector 5975 using the same column.

Characterisation: Size and shape of initial NPs were examined by transmission electron microscopy (TEM) using a ZEISS LIBRA 120, operating at 120 kV. Structural and compositional characterization of the nanocomposites were analysed by high resolution TEM (HRTEM) and high angle annular dark field (HAADF) scanning TEM (STEM) using a field emission gun FEI™ Tecnai F20 microscope at 200 kV with a point-to-point resolution of 0.19 nm. Scanning electron microscopy (SEM) analysis was done in a ZEISS Auriga microscope with an energy dispersive X-ray spectroscopy (EDS) detector at 20 kV to study the chemical composition of NPs. For SEM characterization, NPs were dissolved in chloroform and were drop casted on silicon substrates. X-ray power diffraction (XRD) patterns were obtained on a Bruker AXS D8 Advance diffractometer, using CuK radiation (λ = 1.5406 Å), operating at 40 kV and 40 mA, and with a LynxEye linear position-sensitive detector used in reflection geometry. For XRD characterization, samples were deposited on a Si substrate. Ultraviolet-visible (UV-Vis) spectra

were recorded on a LAMBDA 950 UV-Vis spectrophotometer from PerkinElmer. X-ray photoelectron spectroscopy (XPS) was done on a SPECS system equipped with an Al anode XR50 source operating at 150 mW and a Phoibos 150 MCD-9 detector. The pressure in the analysis chamber was always below 10^{-7} Pa. The area analysed was about 2 mm × 2 mm. The pass energy of the hemispherical analyser was set at 25 eV and the energy step was set at 0.1 eV. Data processing was performed with the CasaXPS program (Casa Software Ltd., UK). Binding energy (BE) values were centered using the C 1s peak at 284.8 eV. The atomic fractions (%) were calculated using peak areas normalized on the basis of acquisition parameters after background subtraction, experimental sensitivity factors and transmission factors provided by the manufacturer. Thermogravimetric analyses (TGA) were performed in the temperature range of 30−500 °C at a heating rate of 10 °C min^{-1} under Ar using a PerkinElmer TGA4000. Nuclear Magnetic Resonance (NMR) measurements were recorded on a Bruker Avance III HD Spectrometer operating at a 1H frequency of 500.26 MHz and equipped with a BBFO-Z probe. The sample temperature was set to 298.2 K. One dimensional (1D) 1H and 2D NOESY (Nuclear Overhauser Effect Spectroscopy) spectra were acquired using standard pulse sequences from the Bruker library. For the quantitative 1D 1H measurements, 64k data points were sampled with the spectral width set to 20 ppm and a relaxation delay of 30 s. NOESY mixing time was set to 300 ms and 4096 data points in the direct dimension for 512 data points in the indirect dimension were typically sampled, with the spectral width set to 10 ppm. Diffusion measurements (2D DOSY) were performed using a double stimulated echo sequence for convection compensation and with monopolar gradient pulses.[44] Smoothed rectangle gradient pulse shapes were used throughout. The gradient strength was varied linearly from 2 to 95% of the probe's maximum value in 64 increments, with the gradient pulse duration and diffusion delay optimized to ensure

a final attenuation of the signal in the final increment of less than 10% relative to the first increment. For 2D processing, the spectra were zero filled until a 4096−2048 real data matrix. Before Fourier transformation, the 2D spectra were multiplied with a squared cosine bell function in both dimensions, the 1D spectra were multiplied with an exponential window function. The diffusion coefficients were obtained by fitting the appropriate Stejskal-Tanner (ST) equation to the signal intensity decay.[43] Diffusion measurements (2D DOSY) were performed using a double stimulated echo sequence for convection compensation and with monopolar gradient pulses.[44] Smoothed rectangle gradient pulse shapes were used throughout. The gradient strength was varied linearly from 2-95% of the probe's maximum value (calibrated at 50.2 G/cm) in 64 steps, with the gradient pulse duration and diffusion delay optimized to ensure a final attenuation of the signal in the final increment of less than 10% relative to the first increment. The diffusion coefficients were obtained by fitting the Stejskal-Tanner (ST) equation to the signal intensity decay. For the pulse sequence at hand, the ST equation is:[43]

$$I = I_0 e^{-D\gamma^2\delta^2 g^2\left(\Delta - \frac{\delta}{3}\right)}$$

with the gyromagnetic ratio of the observed 1H nucleus γ, the gradient pulse length δ, the gradient strength g, the diffusion time Δ and the diffusion coefficient D.

RESULTS AND DISCUSSION

Structural and chemical properties of Pd_2Sn and Au-Pd_2Sn NRs

Representative TEM micrographs of rod-shaped Pd_2Sn NPs with three different sizes (10 ± 2 nm × 4 ± 1 nm; 26 ± 2 nm × 9 ± 1 nm; 40 ± 5 nm × 11 ± 2 nm) produced following the methodology

detailed in the experimental section are shown in Figure 1a, 1c, 1e. NRs showed narrow size distributions and no apparent aggregation.

Au-Pd_2Sn heteronanostructures were produced by injecting, at room temperature, a solution containing 0.02 mmol of $AuCl_3$ in 50 µl of OAm and 2 ml of ODE into 5 mL of a toluene dispersion of Pd_2Sn NRs (5 mg/mL) under strong stirring. After 60 min reaction, multiple Au dots with average size of ca. 2 nm were grown along the whole NR surface for the larger NRs and preferentially at the NR ends in the smallest ones (Figures 1b, 1d, 1f). Figure 1g shows the size distribution histograms of the smallest Pd_2Sn (10 ± 2 nm) and Au-Pd_2Sn NRs produced. Due to the preferential growth of the Au domains at the NR tips, a slight increase of the NR length was obtained in this sample, from 10 ± 2 nm × 4 ± 1 nm to 12 ± 2 nm × 4 ± 1 nm. EDX spectra of single Au-Pd_2Sn NRs confirmed the presence of the three elements, Pd, Sn and Au (Figure 2a). Moreover, UV-vis spectroscopy showed the disappearance of the characteristic Au plasmonic peak, suggesting a strong electronic interaction between Au and Pd_2Sn nanodomains (Figure 1h). Different amounts of Au stock solution resulted in proportional contents of Au on the surface of Pd_2Sn NRs (Figure S1, table 1). However, too high amounts, >0.04 mmol, yielded a large concentration of Au NPs homogeneously nucleated in the solution.

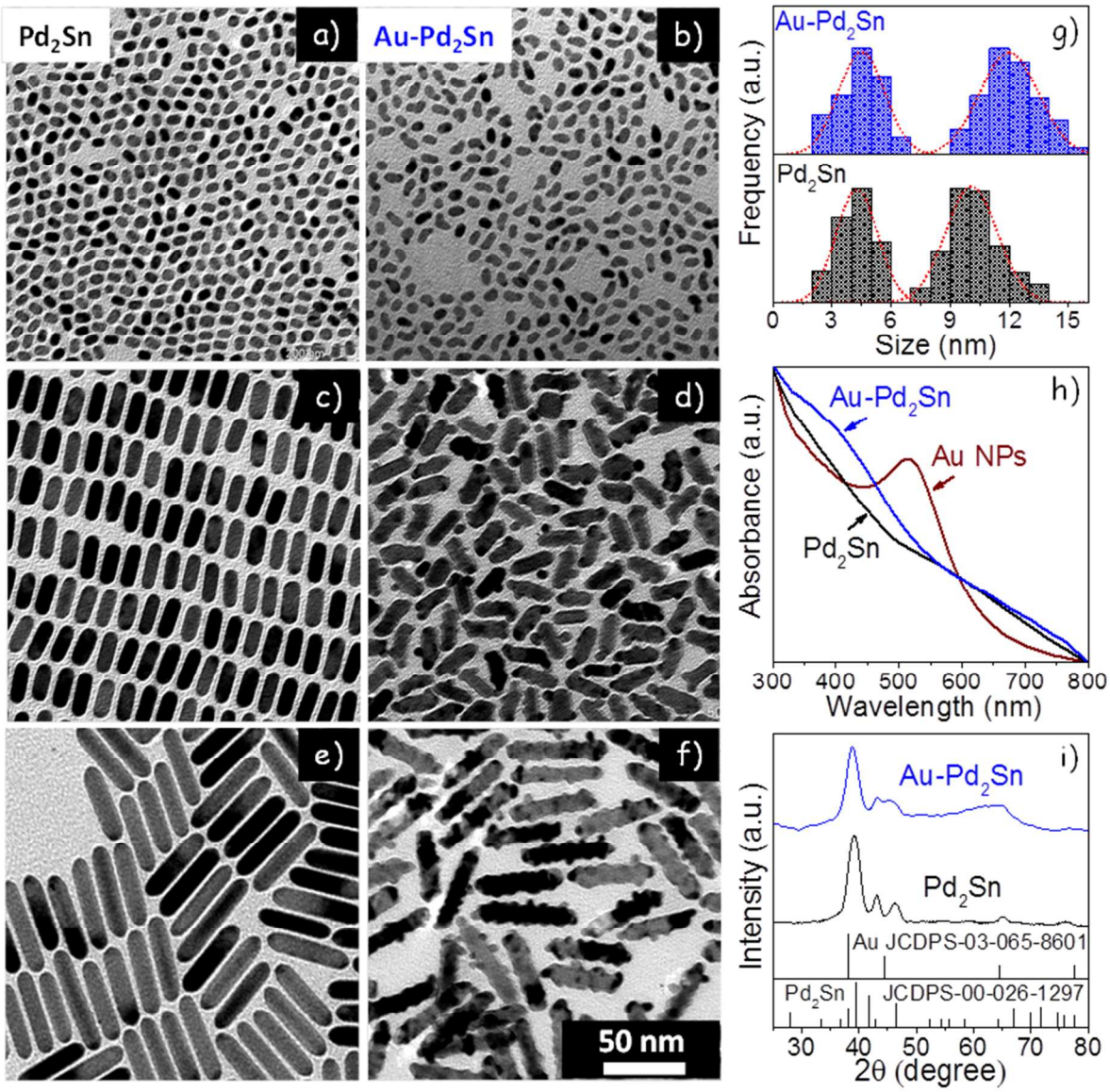

Figure 1. a)-f) TEM micrographs of Pd_2Sn (a, c, e) and Au-Pd_2Sn (b, d, f) NRs with three different sizes: 10 ± 2 nm × 4 ± 1 nm (a, b); 26 ± 2 nm × 9 ± 1 nm (c, d); 40 ± 5 nm × 11 ± 2 nm (e, f). All TEM micrographs have the same scale. g) Size distribution histograms of the smallest Pd_2Sn and Au-Pd_2Sn NRs. h) UV-vis spectra of colloidal 3.5 nm Au NPs (produced by reducing $AuCl_3$ in the absence of Pd_2Sn NRs), 10 nm Pd_2Sn NRs and 12 nm Au-Pd_2Sn NRs (produced from 10 nm Pd_2Sn NRs). i) XRD patterns of 10 nm Pd_2Sn NRs and 12 nm Au-Pd_2Sn NRs, including reference patterns for Pd_2Sn and Au.

HAADF-STEM images of the 12 nm Au-Pd_2Sn NRs further confirmed the presence of Au dots at the Pd_2Sn NR tips, as deduced by the brighter dots associated to the higher Z contrast of Au (Figure 2). Even though most of the NRs showed the presence of Au in just one tip, a few contained Au on both sides of the NR while a few other displayed no contrast difference. XRD patterns showed Pd_2Sn NRs to have an orthorhombic crystal structure (JCPDS No. 00-026-1297). The Au XRD reflections were mostly hidden by the Pd_2Sn peaks, but slight shoulders at $2\theta = 44.5^{o}$ and 64.5^{o} and a shift of the main Pd_2Sn diffraction peak to lower angles suggested the presence of Au crystalline domains (Figure 1i). HRTEM analysis confirmed the orthorhombic crystal structure of Pd_2Sn NRs (space group Pnma) with a = 5.65 Å, b = 4.31 Å and c = 8.12 Å, showed the [010] as the NR growth direction and revealed the presence of Au crystal domains at the Pd_2Sn NR tips (Figure 2c). The Au crystal phase was identified as cubic Fm-3m with a = b = c = 4.09 Å. Within this face, the Au{111} and Pd_2Sn{210} planes, as well as Au{002} and Pd_2Sn{020} present almost identical lattice parameters, which allowed both structures to form almost perfect epitaxy.

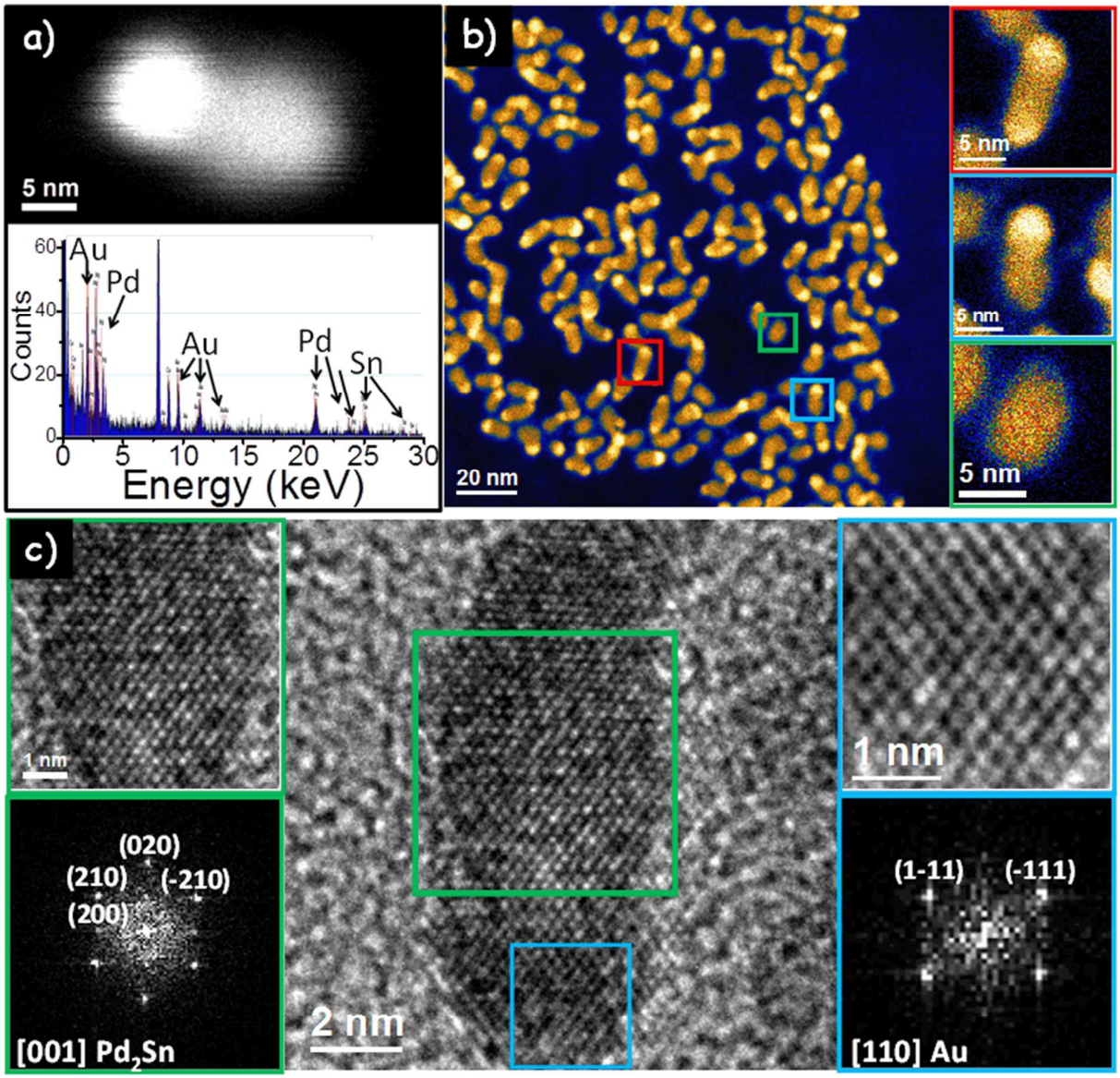

Figure 2. a) HAADF-STEM image of a single Au-Pd_2Sn NR and its corresponding EDX spectrum. b) Coloured HAADF-STEM image of Au- Pd_2Sn NRs and details of three different NRs, one containing higher contrast dots at both ends, another at only one end (most common case) and another without any higher contrast region. c) HRTEM micrograph of a single Au-Pd_2Sn NR, details of the squared regions and their corresponding power spectra.

Within its experimental error, EDX analysis of 10 nm Pd_2Sn NRs showed the atomic ratio of Pd and Sn to be consistent with stoichiometric Pd_2Sn ([Pd]/[Sn] = 2.0 ± 0.1). However, with the

introduction of Au, higher Pd ratios were systematically obtained as detailed in Table 1. We associate this experimental observation to a galvanic replacement of Sn by Au. When adding $AuCl_3$ to the solution containing Pd_2Sn NRs, Au^{3+} ions in solution were reduced to Au^+ or even Au^0 at the NR surface through the simultaneous oxidation of Sn or Sn^{2+} ions to Sn^{4+} and the subsequent solvation of Sn^{4+} ions in the solution containing the remaining chlorine ions. Au^+ could be also further reduced to Au^0 through charge transfer from Pd atoms (Figure 3a).[23]

Table 1. Atomic ratios of 10 nm Pd_2Sn and 12 nm Au-Pd_2Sn NRs as obtained by EDX and XPS analyses, and atomic percentage of each oxidation state as obtained from the fitting of the XPS spectra.

	EDX		XPS								
$[AuCl_3]$ M	[Pd]/[Sn]	[Au]/[Pd]	[Pd]/[Sn]	[Au]/[Pd]	Pd^0 at%	Pd^{2+} at%	Sn^0 at%	Sn^{2+} at%	Sn^{4+} at%	Au^0 at%	$Au^{\delta+}$ at%
-	2.0	-	1.25	-	79.4	20.6	21.7	70.2	8.0	-	-
0.01	2.2	0.07									
0.02	2.3	0.14	5.5	0.5	86.2	13.8	18.4	81.7		61.9	38.1
0.04	2.4	0.26									

To further clarify the composition and oxidation states of the different elements within Pd_2Sn and Au-Pd_2Sn NRs, samples were analysed using XPS (Figure 3b-f). In 10 nm Pd_2Sn NRs, the atomic ratio of Pd and Sn was measured as [Pd]/[Sn] = 1.25, pointing at a surface segregation of Sn. However, this ratio was much higher in 12 nm Au-Pd_2Sn NRs, up to [Pd]/[Sn] = 5.5 when using a 0.02 M $AuCl_3$ concentration to grow the Au tips (Table 1). This experimental result further points toward a galvanic replacement of surface Sn by Au. Fitting each region of the XPS spectra, it could be observed that in Pd_2Sn and Au-Pd_2Sn NRs the deconvolution of the Pd 3d spectra indicated the presence of two Pd oxidation states, a dominant Pd^0 state with a doublet at around 335.6 eV (Pd $3d_{5/2}$) and 340.9 eV (Pd $3d_{3/2}$), and a Pd^{2+} state with a doublet at 337.6 eV

(Pd $3d_{5/2}$) and 342.9 eV (Pd $3d_{3/2}$). With the Au introduction, these two doublets were slightly shifted to lower binding energies ($\Delta E = -0.5$ eV) and an increase of the Pd^0 contribution was observed. Larger changes were obtained in the Sn 3d spectral region, which showed three main Sn contributions in Pd_2Sn NRs: a main Sn^{2+} (486.3 eV and 494.9 eV) and minor Sn^{4+} (488.4 eV and 496.8 eV) and Sn^0 (484.8 eV and 493.3 eV) components. Oxidized Sn phases, related either to the Sn reaction with oxygen or its coordination with ligands, are a common observation on the surface of Pd-Sn and Pt-Sn alloys.[45,46] With the introduction of Au, on top of the decrease of the Sn signal described above, the main Sn^{2+} contribution was further oxidized, shifting its doublet peak position more than 1 eV toward higher binding energies. Finally, the deconvolution of the Au 4f spectrum in Au-Pd_2Sn showed 2 doublets. The major contribution corresponded to metallic Au (83.3 eV and 87.0 eV), and the minor contribution, at higher binding energy (84.5 eV and 88.2 eV), indicated the presence of positively charged gold atoms, $Au^{\delta+}$, attributed to Au surface atoms with different environments.

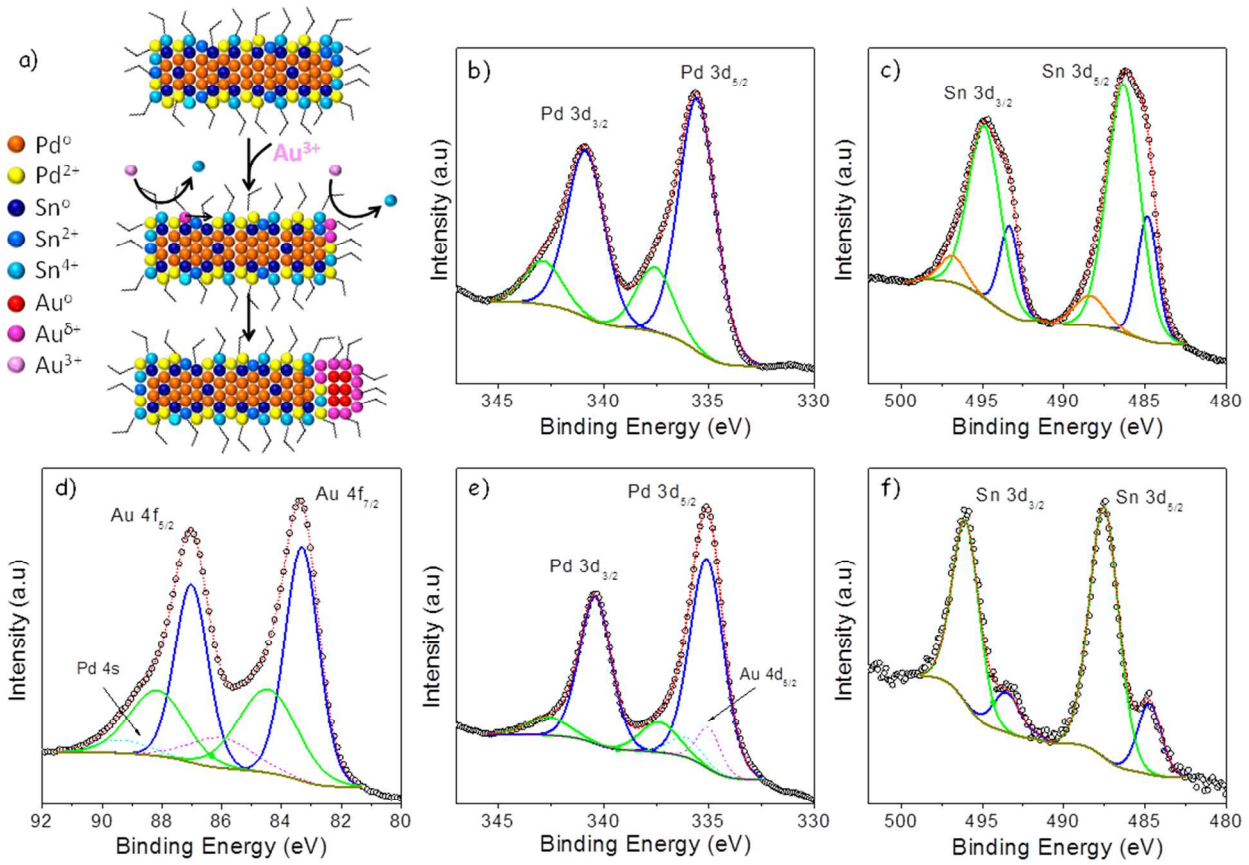

Figure 3. a) Scheme of the proposed Au-Pd_2Sn formation mechanism. b-f) Detailed regions of the XPS spectra of 10 nm Pd_2Sn (b, c) and 12 nm Au-Pd_2Sn NRs (d-f): Pd 3d (b,e), Sn 3d (c,f) and Au 4f (d), as indicated within each graph.

The Pd_2Sn NR surface chemistry was further elucidated by thermogravimetric analysis and solution ^{1}H NMR after thoroughly washing the NRs. Thermogravimetric analysis showed the presence of a 12% of organics in 10 nm Pd_2Sn NRs (Figure S2). In the solution ^{1}H NMR spectra, the resonance at chemical shift around 5.3 ppm characteristic of the alkene group indicated the presence of OAm (Figure S3 and S4a). The alkene group displayed slightly shifted sharp resonances in the ^{1}H NMR spectra, in contrast to the broad resonances typically characteristic of tightly bound ligands.[42] In parallel, NOESY spectra presented negative cross peaks corroborating the interaction of OAm with the Pd_2Sn surface (Figure S4b). These data

pointed toward the possibility of a highly dynamic surface stabilization, as previously reported for other systems.[47,48] Hence, we studied the diffusion coefficient of our system (NR plus the ligand shell) using DOSY experiments. From DOSY data (Figure S5), a diffusion coefficient of 120 ± 12 $\mu m^2 s^{-1}$ was obtained for 26 nm Pd_2Sn NRs. The diffusion coefficient calculated using the theoretical model of Mansfield and Douglas[49] for 26 nm NRs with rounded ends was 26 $\mu m^2 s^{-1}$. The much larger diffusion coefficient experimentally measured was ascribed to a highly dynamic binding of OAm on the Pd_2Sn NRs surface.

Hydrogenation reactions

The exploration of the catalytic potential of Pd_2Sn and Au-Pd_2Sn NRs was started with the hydrogenation of styrene to ethylbenzene (Table 2). Pd_2Sn NRs were active in the hydrogenation reaction when dichloromethane was used as solvent and H_2 pressure was set at 3 bar. 10 nm Pd_2Sn NRs achieved conversions above 70% at large substrate loadings (100 g styrene/g Pd_2Sn) even under mild reaction conditions (25 °C, Table 2, entry 1). Larger Pd_2Sn NRs systematically resulted in lower activities (Table 2, entry 2). We associate this experimental result to their lower surface-to-bulk ratio and possibly to their reduced density of potentially active sites such as tips. Thus 10 nm Pd_2Sn NRs were used for all following catalytic tests.

Activity was lower at 1 bar of H_2 (Table 2, entry 4) and when using methanol as solvent (Table 2, entry 5) due to the low colloidal stability of the NRs in this solvent. Even at much harsher conditions (Table 2, entry 6), the reaction yielded just ethylbenzene, without any trace of phenyl group hydrogenation. Without solvent, in neat styrene (Table 2, entry 7), the highest TOF values up to 286 h-1 were reached. Overall, TOF values compared favorably to related nanosystems making use of other metals.[50]

Table 2. Results of the styrene hydrogenation with Pd_2Sn NRs.

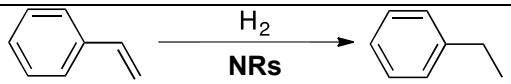

Entry	*Catalyst (size/nm)*	*Solvent*	*T/ºC*	*P/bar*	*t/h*	*Loading*[a]	*Conv/%*	*TOF/h*$^{-1}$
1	Pd_2Sn (10 x 4)	DCM	25	3	1	100	73.3	114
2	Pd_2Sn (40 x 12)	DCM	25	3	1	99	53.3	84
3	Au-Pd_2Sn (12 x 4)	DCM	25	3	1	100	48.3	86
4	Pd_2Sn (10 x 4)	DCM	25	1	1	104	12.8	21
5[b]	Pd_2Sn (10 x 4)	MeOH	25	3	1	103	58.0	96
6	Pd_2Sn (10 x 4)	Toluene	70	50	4	30	100	–
7[c]	Pd_2Sn (10 x 4)	–	25	3	1	436	41.3	287

[a]g styrene/g NRs. [b]NRs were poorly soluble in methanol. [c]The reaction was carried out in neat styrene.

Tables 3 and 4 show results obtained from the hydrogenation of 1-octene and alkynes, namely phenylacetylene and 1-octyne, under the optimized conditions set with styrene. In the hydrogenation of 1-octene, apart from the hydrogenated product, octane, isomerisation of the substrate to the two geometric isomers of 2-octene was observed. This isomerization depends on the sequence of insertion and β-hydride elimination on the NR surface (Scheme S1) Similar results and tendencies were obtained for the hydrogenation of 1-octyne. On the other hand, in the hydrogenation of phenylacetylene, very little amounts of ethylbenzene were formed, evidencing the higher reactivity of phenylacetylene compared to styrene in hydrogenation.

Table 3. Results of 1-octene hydrogenation with Pd_2Sn and Au-Pd_2Sn NRs.[a]

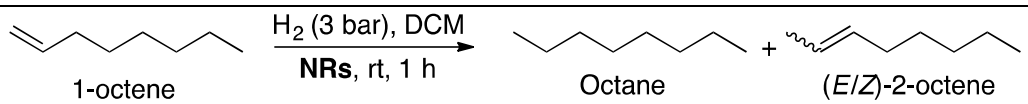

Catalyst	*Conv/%*	*TOF/h*$^{-1}$	*Selectivity/%*		
			Octane	*(E)-2-octene*	*(Z)-2-octene*
Pd_2Sn	70.6	110.2	52.7	27.6	19.7
Au-Pd_2Sn	98.1	157.2	56.7	32.7	10.6

[a] The catalyst loading (g 1-octene/g NRs) was 106.

In terms of the Au effect on hydrogenation reactions, Pd_2Sn NRs were considerably more active in the hydrogenation of styrene than Au-Pd_2Sn NRs, whereas the opposite trend was observed for 1-octene. The non-conjugated nature of the double bond and the lesser steric shielding of 1-octene compared to styrene could explain this result. In contrast, the differences in performance were less important for phenylacetylene and 1-octyne, with Au-Pd_2Sn being more active for both substrates. These trends could be understood by the known alkynophilicity of Au.[39–41,51] The high electron rich character of the triple bond probably hid the effect of the substituent. It should be mentioned that all the comparisons carried out between Pd_2Sn and Au-Pd_2Sn NRs were based on results obtained from the exact same batch of Pd_2Sn NRs.

Table 4. Results of alkyne hydrogenation with Pd_2Sn and Au-Pd_2Sn NRs.[a]

Phenylacetylene Styrene Ethylbenzene

Catalyst	*Conv/%*	*TOF/h^{-1}*	*Selectivity/%*	
			Styrene	*Ethylbenzene*
Pd_2Sn	46.4	78.9	96.6	3.4
Au-Pd_2Sn	54.8	90.7	96.7	3.3

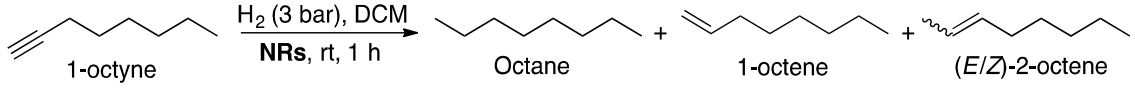

1-octyne Octane 1-octene (*E*/*Z*)-2-octene

NR	*Conv/%*	*TOF/h^{-1}*	*Selectivity/%*			
			Octane	*1-octene*	*(E)-2-octene*	*(Z)-2-octene*
Pd_2Sn	47.4	75.5	0.0	98.1	1.9	0.0
Au-Pd_2Sn	58.7	93.9	0.7	94.4	4.0	0.9

[a]The catalyst loading (g alkyne/g NRs) was 106.

Sonogashira coupling reactions

Pd_2Sn and Au-Pd_2Sn NR performance in the Sonogashira reaction between phenylacetylene (PhA) and iodobenzene (phenyl iodide, PhI) to give diphenylacetylene (tolan) are displayed in Table 5. Using Pd_2Sn NRs and K_2CO_3 as base (Table 5, entries 1-4), very high conversions could

be attained at 2 h (Table 5, entry 2). The reaction yielded mainly tolan, although products 1 and 1' were also formed. Both products were analyzed by GC-MS, providing a peak at m/z of 280 units, what proved that they were isomeric. These compounds arose from the condensation of two molecules of PhA and one molecule of PhI, which gave a pair of geometric isomers of a 1,3-enyne (Figure 4). The decrease of the catalyst loading (Table 5, entry 3) produced a drop on the conversion and selectivity to tolan. The calculated TOF values were similar to those obtained previously from related Pd-nanosytems.[9]

When the base was changed to KOH (Table 5, entries 5-8), activities significantly increased, achieving full conversion at 1 h (Table 5, entries 5 and 7). However, the selectivity toward tolan was not improved, because apart from 1 and 1', trans-stilbene (tSt) was also produced. This compound is the product of the formal addition of H_2 to tolan. Interestingly, not even trace amounts of cis-stilbene (cSt) were detected. Additionally, in all the essays with KOH, a trace quantity of triphenylethene (TPE) was formed, which arised from the combination of a molecule of PhA and two molecules of PhI.

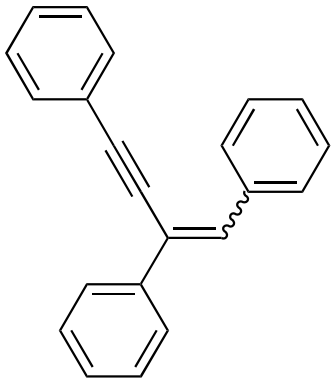

1 + 1'

Figure 4. Proposed structures of 1 and 1'.

The recyclability of the Pd_2Sn NRs in the Sonogashira reactions was studied by precipitating the nanoparticles by centrifugation and using them in successive runs. To the recovered NRs, a new batch of fresh reagents was added to carry out a second catalytic run under the same conditions. A 10 % drop in the conversion in the first run, but no change in the selectivity (Figure S6). We associate this drop to non-full recovery of the material in each precipitation step. A partial NR aggregation during the recovery was also observed (Figure S7), which likely reduced the NR catalytic activity (see SI for details).

Table 5. Results of Sonogashira with Pd_2Sn and Au-Pd_2Sn NRs.

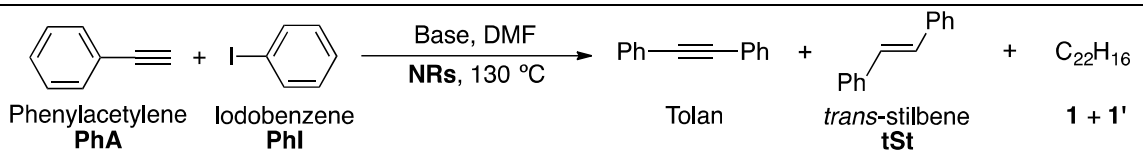

Entry	*Catalyst*	*Base*	*t/h*	*Conv/%*	*Tolan/%*	***tSt/%***	***1+1'/%***
1	Pd_2Sn	K_2CO_3	1.0	47.2	70.6	–	29.4
2	Pd_2Sn	K_2CO_3	2.0	97.3	65.7	–	34.7
3[a]	Pd_2Sn	K_2CO_3	1.0	10.9	40.6	–	59.4
4	Au-Pd_2Sn	K_2CO_3	1.0	20.9	60.9	–	39.1
5	Pd_2Sn	KOH	1.0	100	60.8	17.6	21.6
6	Pd_2Sn	KOH	0.5	88.3	66.7	17.9	15.4
7	Au-Pd_2Sn	KOH	1.0	100	65.0	17.0	18.0
8	Au-Pd_2Sn	KOH	0.5	100	67.0	14.1	18.9

[a]5.3 mg of NR were used.

An interesting aspect of the catalytic runs was the unexpected formation of the products tSt, 1, 1' and TPE. To shed light into the formation of these products, we carried out a set of experiments at different conditions (Table 6). It was found that reducing the concentration of PhI fivefold with respect to the 0.1 M used in previous experiments improved the selectivity to tolan (Table 6, cf. entries 1 with 2 and 4 with 5) by diminishing the quantity of 1 and 1' or eliminating it completely in the case of Au-Pd_2Sn NRs (Table 6, entry 4). Unexpectedly, with Pd_2Sn NRs, increasing the PhI concentration to 0.5 M (Table 6, entry 3) resulted in no trace of tolan but the

formation of new products cSt, 1,2-diphenylethane (DPE), TPE and 2 (Figure S8). A similar result was obtained with Au-Pd_2Sn NRs (Table 6, entry 6), but in this case only traces of DPE were formed, what improved the selectivity toward cSt.

Table 6. Effect of the concentration on the Sonogashira reaction with NRs.[a]

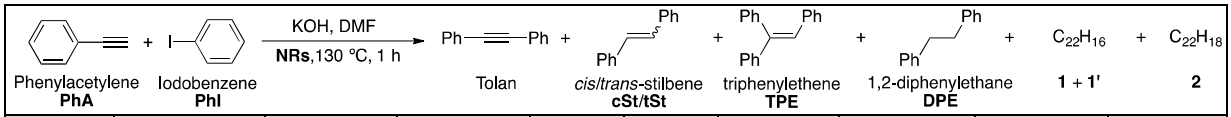

Entry	*NRs*	*[PhI]/M*	*Tolan/%*	***tSt**/%*	***cSt**/%*	***TPE**/%*	***DPE**/%*	***1+1'**/%*	***2**/%*
1	Pd_2Sn	0.02	66.7	16.9	–	–	–	16.4	–
2	Pd_2Sn	0.1	60.8	17.6	–	–	–	21.6	–
3	Pd_2Sn	0.5	–	10.1	49.2	6.2	9.8	15.2	9.5
4	Au-Pd_2Sn	0.02	88.7	11.3	–	–	–	–	–
5	Au-Pd_2Sn	0.1	65.0	17.0	–	–	–	18.0	–
6	Au-Pd_2Sn	0.5	–	11.9	63.7	3.8	–	17.5	3.1

DPE and 2 can be obtained from the formal addition of hydrogen to St and to 1/1' respectively, whereas St comes from the formal addition of hydrogen to tolan. To understand the origin of the reduced products and the different selectivity of Pd_2Sn and Au-Pd_2Sn NRs, a sample of tolan was subjected to the catalytic conditions of the Sonogashira coupling (Table 7). Under Sonogashira conditions, Pd_2Sn and Au-Pd_2Sn NRs catalysed the reduction of tolan to St, but not to DPE. The reduction was quite selective to the formation of cSt, as it happened when the Sonogashira coupling was carried out at high concentration (Table 6). As no trace of 1/1' or 2 was detected, it was concluded that the formation of these molecules needed PhI and PhA. Au-Pd_2Sn NRs were less active for the reduction of tolan, possibly due to the stronger adsorption of the triple bond to Au.[39–41,51]

Table 7. Results of tolan reduction with NRs.

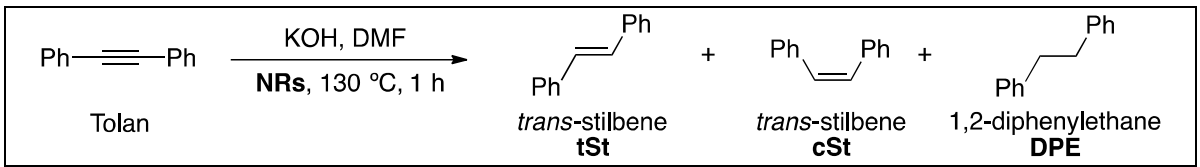

NR[a]	*Tolan/%*	***tSt**/%*	***cSt**/%*	***DPE**/%*

Pd_2Sn	–	10.7	89.3	–
Au-Pd_2Sn	33.6	7.1	59.2	–

From the above data, a mechanism for the formation of the different products could be envisaged (Scheme 1). The formation of the expected tolan through Sonogashira coupling (left in Scheme 1) involved oxidative addition of PhI, transmetallation with PhA and reductive elimination. The reduction of tolan catalyzed by the Pd_2Sn or Au-Pd_2Sn NRs lead to the formation of mainly cSt as shown by the data of Table 6 at high concentration and also by experiments of Table 7. An alternative mechanism (right in Scheme 1) might start with an initial insertion of PhA into the Ph–NR bond forming an intermediate. From this intermediate, 1, 1', St and TPE could be produced by functionalization of the NRs and reductive elimination (see Scheme S2). It is interesting to note that by this mechanism, tSt, the most thermodynamically stable compound, is mainly formed as shown in Tables 5 and 6.

Although the reduction of both St isomers produces DPE, the selectivity to cSt observed when

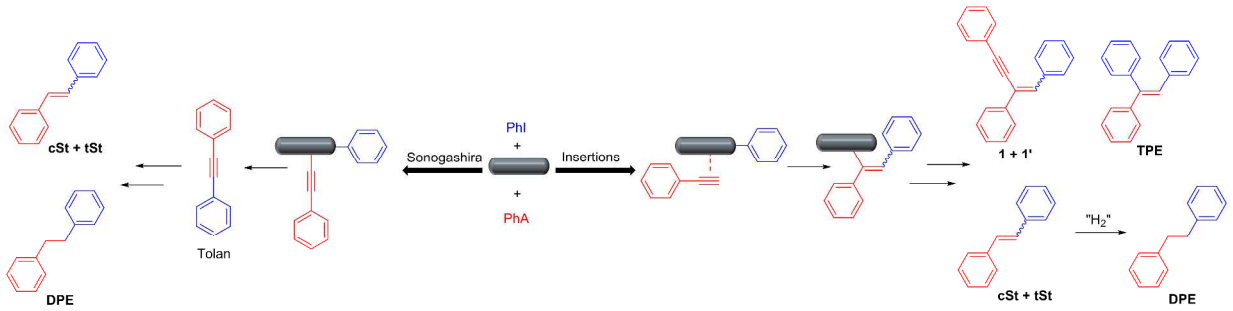

performing the reactions at high concentration (Table 6) suggested that most of the DPE was formed by the reduction of cSt, shown in the left-hand side of Scheme 1.

Scheme 1. Mechanisms for the formation of the different products of the Sonogashira coupling reaction between PhI and PhA.

Under the Sonogashira catalytic conditions the formal addition of a molecule of hydrogen to tolan, St, 1 and 1' was observed. This pointed out that molecular hydrogen, formed by decomposition of DMF,[52,53] was probably involved in the reductions. To explore the origin of the added hydrogen atoms an experiment with DMF-d_7 was performed (See Supporting Information). The detection of a mixture of hydrogenated and deuterated reduction products indicated that the solvent provided the required H or D atoms.[52,53]

CONCLUSIONS

Au nanodomains were grown at the surface of Pd_2Sn NRs through a process involving a galvanic replacement with Sn ions. The surface chemistry of Pd_2Sn and Au-Pd_2Sn NRs was characterized by XPS and NMR. XPS results evidenced an electron donation from the Pd_2Sn NR to the Au tips. Both Pd_2Sn and Au-Pd_2Sn NRs were found to be very active in the hydrogenation of aromatic and aliphatic alkenes and alkynes under mild conditions. While Pd_2Sn NRs were more active in the hydrogenation of styrene, Au-Pd_2Sn NRs performed better for the hydrogenation of alkynes, probably due to their aurophilicity. Pd_2Sn and Au-Pd_2Sn NRs were also active in the Sonogashira coupling between PhA and PhI to yield tolan in good selectivity, especially with Au-Pd_2Sn NRs, when the reaction was performed at high dilution. Interestingly, St was produced at higher concentration either by reduction of tolan or by a mechanism involving insertion of PhA into the NR-Ph bond. In this regard, the production of St can be considered a cascade or tandem reaction, which was performed with a better selectivity using Au-Pd_2Sn NRS as a catalyst. Additionally, the deuterated experiments confirmed that the solvent (DMF) played a role in this cascade reaction. We are currently investigating the implications of this methodology with other substrates.

AUTHOR INFORMATION

Corresponding Authors

*E-mail: arnald.grabulosa@qi.ub.es (A.G.).

*E-mail: acabot@irec.cat (A.C.).

Authors Contributions

‡ These authors contributed equally

Notes

The authors declare no competing financial interest.

ACKNOWLEDGEMENTS

This work was supported by the European Regional Development Funds and the Spanish MINECO projects ENE2013-46624-C4-3-R, MAT2014-59961-C2-2-R and CTQ2015-65040-P. Z.L. and X.Y. thanks the China Scholarship Council for scholarship support. M.I. thanks AGAUR for Beatriu de Pinós postdoctoral grant (2013 BP-A00344). J.L. is Serra Húnter Fellow and is grateful to ICREA Academia program. Authors also acknowledge the funding from Generalitat de Catalunya 2014 SGR 1638. SMS acknowledges funding from "Programa Internacional de Becas "la Caixa - Severo Ochoa". ICN2 acknowledges support from the Severo Ochoa Program (MINECO, Grant SEV-2013-0295). Part of the present work has been performed in the framework of Universitat Autònoma de Barcelona Materials Science PhD program. We would like to thank Michaela Meyns for fruitful discussions.

REFERENCES

(1) Guczi, L. Mechanism of Reactions on Multimetallic Catalysts. *J. Mol. Catal.* **1984**, *25*, 13–29.

(2) Mata, J. A.; Hahn, F. E.; Peris, E. Heterometallic Complexes, Tandem Catalysis and Catalytic Cooperativity. *Chem. Sci.* **2014**, *5*, 1723–1732.

(3) Buchwalter, P.; Rosé, J.; Braunstein, P. Multimetallic Catalysis Based on Heterometallic Complexes and Clusters. *Chem. Rev.* **2015**, *115*, 28–126.

(4) Shibasaki, M.; and Yamamoto, Y. Multimetallic Catalysts in Organic Synthesis, Wiley-VCH 2004.

(5) Jia, C. J.; Schüth, F. Colloidal Metal Nanoparticles as a Component of Designed Catalyst. *Phys. Chem. Chem. Phys.* **2011**, *13*, 2457–2487.

(6) Astruc, D.; Lu, F.; Ruiz Aranzaes, J. Nanoparticles as Recyclable Catalysts: The Frontier between Homogeneous and Heterogeneous Catalysis. *Angew. Chem. Int. Ed*. **2005**, *44*, 7852-7872

(7) Balanta, A.; Godard, C.; Claver, C. Pd Nanoparticles for C-C Coupling Reactions. *Chem. Soc. Rev.* **2011**, *40*, 4973–4985.

(8) Astruc, D. Palladium Nanoparticles as Efficient Green Homogeneous and Heterogeneous Carbon-Carbon Coupling Precatalysts: A Unifying View. *Inorg. Chem.* **2007**, *46*, 1884–1894.

(9) Chu, Y. T.; Chanda, K.; Lin, P. H.; Huang, M. H. Aqueous Phase Synthesis of Palladium Tripod Nanostructures for Sonogashira Coupling Reactions. *Langmuir* **2012**, *28*, 11258–11264.

(10) Pérez-Lorenzo, M. Palladium Nanoparticles as Efficient Catalysts for Suzuki Cross-Coupling Reactions. *J. Phys. Chem. Lett.* **2012**, *3*, 167–174.

(11) De Roo, J.; Van Driessche, I.; Martins, J. C.; Hens, Z. Colloidal Metal Oxide Nanocrystal Catalysis by Sustained Chemically Driven Ligand Displacement. *Nat. Mater.* **2016**, *15*, 517–521.

(12) Gilroy, K. D.; Ruditskiy, A.; Peng, H. C.; Qin, D.; Xia, Y. Bimetallic Nanocrystals: Syntheses, Properties, and Applications. *Chem. Rev.* **2016**, *116*, 10414–10472.

(13) Flox, C.; Rubio-Garcia, J.; Nafria, R.; Zamani, R.; Skoumal, M.; Andreu, T.; Arbiol, J.; Cabot, A.; Morante, J. R. Active Nano-CuPt3 Electrocatalyst Supported on Graphene for Enhancing Reactions at the Cathode in All-Vanadium Redox Flow Batteries. *Carbon.* **2012**, *50*, 2372–2374.

(14) Yu, X.; Shavel, A.; An, X.; Luo, Z.; Ibáñez, M.; Cabot, A. Cu2ZnSnS4-Pt and Cu2ZnSnS4-Au Heterostructured Nanoparticles for Photocatalytic Water Splitting and Pollutant Degradation. *J. Am. Chem. Soc.* **2014**, *136*, 9236–9239.

(15) Nafria, R.; Genç, A.; Ibáñez, M.; Arbiol, J.; Ramírez De La Piscina, P.; Homs, N.; Cabot, A. Co-Cu Nanoparticles: Synthesis by Galvanic Replacement and Phase Rearrangement during Catalytic Activation. *Langmuir* **2016**, *32*, 2267–2276.

(16) Luo, Z.; Ibáñez, M.; Antolín, A. M.; Genç, A.; Shavel, A.; Contreras, S.; Medina, F.; Arbiol, J.; Cabot, A. Size and Aspect Ratio Control of Pd2Sn Nanorods and Their Water Denitration Properties. *Langmuir* **2015**, *31*, 3952–3957.

(17) Xia, X.; Wang, Y.; Ruditskiy, A.; Xia, Y. 25th Anniversary Article: Galvanic Replacement: A Simple and Versatile Route to Hollow Nanostructures with Tunable and Well-Controlled Properties. *Adv. Mater.* **2013**, *25*, 6313–6332.

(18) Oh, M.; Yu, T.; Yu, S.; Lim, B.; Ko, K.; Willinger, M.; Seo, D.; Kim, B.; Cho, M.; Park, J.; Kang, K.; Sung, Y.; Pinna, N.; Hyeon, T. Galvanic Replacement Reactions in Metal Oxide Nanocrystals. *Science* **2013**, *340*, 964–968.

(19) Anderson, B. D.; Tracy, J. B. Nanoparticle Conversion Chemistry: Kirkendall Effect, Galvanic Exchange, and Anion Exchange. *Nanoscale* **2014**, *6*, 12195–12216.

(20) Da Silva, A. G. M.; Rodrigues, T. S.; Haigh, S. J.; Camargo, P. H. C. Galvanic Replacement Reaction: Recent Developments for Engineering Metal Nanostructures towards Catalytic Applications. *Chem. Commun.* **2017**, *53*, 7135–7148.

(21) Liu, X.; Astruc, D. From Galvanic to Anti-Galvanic Synthesis of Bimetallic Nanoparticles and Applications in Catalysis, Sensing, and Materials Science *Adv. Mater.* **2017**, *29*, 1605305.

(22) Cobley, C. M.; Xia, Y. Engineering the Properties of Metal Nanostructures via Galvanic Replancement Reactions. *Mater Sci Eng R Rep.* **2010**, *70*, 44–62.

(23) Krylova, G.; Giovanetti, L. J.; Requejo, F. G.; Dimitrijevic, N. M.; Prakapenka, A.;

Shevchenko, E. V. Study of Nucleation and Growth Mechanism of the Metallic Nanodumbbells. *J. Am. Chem. Soc.* **2012**, *134*, 4384–4392.

(24) Kwon, S. G.; Krylova, G.; Phillips, P. J.; Klie, R. F.; Chattopadhyay, S.; Shibata, T.; Bunel, E. E.; Liu, Y.; Prakapenka, V. B.; Lee, B.; et al. Heterogeneous Nucleation and Shape Transformation of Multicomponent Metallic Nanostructures. *Nat. Mater.* **2015**, *14*, 215–223.

(25) *The Handbook of Homogeneous Hydrogenation;* de Vries, J. G., Elsevier, C. J., Ed.; Wiley-VCH Verlag GmbH, 2008.

(26) Karak, M.; Barbosa, L. C. A.; Hargaden, G. C. Recent Mechanistic Developments and next Generation Catalysts for the Sonogashira Coupling Reaction. *RSC Adv.* **2014**, *4*, 53442–53466.

(27) Freakley, S. J.; He, Q.; Harrhy, J. H.; Lu, L.; Crole, D. A.; Morgan, D. J.; Ntainjua, E. N.; Edwards, J. K.; Carley, A. F.; Borisevich, A. Y.; et al. Palladium-Tin Catalysts for the Direct Synthesis of H_2O_2 with High Selectivity. *Science* **2016**, *351*, 965–968.

(28) Negishi, E.; Anastasia, L. Palladium-Catalyzed Alkynylation. *Chem. Rev.* **2003**, *103*, 1979–2018.

(29) López, N.; Vargas-Fuentes, C. Promoters in the Hydrogenation of Alkynes in Mixtures: Insights from Density Functional Theory. *Chem. Commun.* **2012**, *48*, 1379–1391.

(30) Sales, E. A.; Jove, J.; De Jesus Mendes, M.; Bozon-Verduraz, F. Palladium, Palladium-Tin, and Palladium-Silver Catalysts in the Selective Hydrogenation of Hexadienes: TPR,

Mössbauer, and Infrared Studies of Adsorbed CO. *J. Catal.* **2000**, *195*, 88–95.

(31) Pattamakomsan, K.; Ehret, E.; Morfin, F.; Gélin, P.; Jugnet, Y.; Prakash, S.; Bertolini, J. C.; Panpranot, J.; Aires, F. J. C. S. Selective Hydrogenation of 1,3-Butadiene over Pd and Pd-Sn Catalysts Supported on Different Phases of Alumina. *Catal. Today* **2011**, *164*, 28–33.

(32) Hugon, A.; Delannoy, L.; Louis, C. Catalysts for Selective Hydrogenation of Butadiene in the Presence of an Excess of Alkenes. *Gold Bull.* **2008**, *41*, 127–138.

(33) González-Arellano, C.; Abad, A.; Corma, A.; García, H.; Iglesias, M.; Sánchez, F. Catalysis by gold(I) and gold(III): A Parallelism between Homo- and Heterogeneous Catalysts for Copper-Free Sonogashira Cross-Coupling Reactions. *Angew. Chemie - Int. Ed.* **2007**, *46*, 1536–1538.

(34) De Souza, R. O. M. A.; Bittar, M. S.; Mendes, L. V. P.; Da Silva, C. M. F.; Da Silva, V. T.; Antunes, O. A. C. Copper-Free Sonogashira Reaction Using Gold Nanoparticles Supported on Ce2O3, Nb2O5 and SiO2 under Microwave Irradiation. *Synlett* **2008**, 1777–1780.

(35) Beaumont, S. K.; Kyriakou, G.; Lambert, R. M. Identity of the Active Site in Gold Nanoparticle-Catalyzed Sonogashira Coupling of Phenylacetylene and Iodobenzene. *J. Am. Chem. Soc.* **2010**, *132*, 12246–12248.

(36) Kanuru, V. K.; Kyriakou, G.; Beaumont, S. K.; Papageorgiou, A. C.; Watson, D. J.; Lambert, R. M. Sonogashira Coupling on an Extended Gold Surface in Vacuo: Reaction of Phenylacetylene with Iodobenzene on Au(111). *J. Am. Chem. Soc.* **2010**, *132*, 8081–

8086.

(37) Venkatesan, P.; Santhanalakshmi, J. Designed Synthesis of Au/Ag/Pd Trimetallic Nanoparticle-Based Catalysts for Sonogashira Coupling Reactions. *Langmuir* **2010**, *26*, 12225–12229.

(38) Corma, A.; Juárez, R.; Boronat, M.; Sánchez, F.; Iglesias, M.; García, H. Gold Catalyzes the Sonogashira Coupling Reaction without the Requirement of Palladium Impurities. *Chem. Commun.* **2011**, *47*, 1446–1448.

(39) Corma, A.; Garcia, H. Supported Gold Nanoparticles as Catalysts for Organic Reactions. *Chem. Soc. Rev.* **2008**, *37*, 2096–2126.

(40) García-Mota, M.; Cabello, N.; Maseras, F.; Echavarren, A. M.; Pérez-Ramírez, J.; Lopez, N. Selective Homogeneous and Heterogeneous Gold Catalysis with Alkynes and Alkenes: Similar Behavior, Different Origin. *ChemPhysChem* **2008**, *9*, 1624–1629.

(41) Stratakis, M.; Garcia, H. Catalysis by Supported Gold Nanoparticles: Beyond Aerobic Oxidative Processes. *Chem. Rev.* **2012**, *112*, 4469–4506.

(42) Hens, Z.; Martins, J. C. A Solution NMR Toolbox for Characterizing the Surface Chemistry of Colloidal Nanocrystals. *Chem. Mater.* **2013**, *25*, 1211–1221.

(43) Sinnaeve, D. The Stejskal–Tanner Equation Generalized for Any Gradient Shape—An Overview of Most Pulse Sequences Measuring Free Diffusion. *Concepts Magn Reson Part A* **2012**, *40A*, 39–65.

(44) Connell, M. A.; Bowyer, P. J.; Adam Bone, P.; Davis, A. L.; Swanson, A. G.; Nilsson,

M.; Morris, G. A. Improving the Accuracy of Pulsed Field Gradient NMR Diffusion Experiments: Correction for Gradient Non-Uniformity. *J. Magn. Reson.* **2009**, *198*, 121–131.

(45) Du, W.; MacKenzie, K. E.; Milano, D. F.; Deskins, N. A.; Su, D.; Teng, X. Palladium-Tin Alloyed Catalysts for the Ethanol Oxidation Reaction in an Alkaline Medium. *ACS Catal.* **2012**, *2*, 287–297.

(46) Lee, A. F.; Baddeley, C. J.; Hardacre, C.; Moggridge, G. D.; Ormerod, R. M.; Lambert, R. M.; Candy, J. P.; Basset, J.-M. Structure−Reactivity Correlations in the Catalytic Coupling of Ethyne over Novel Bimetallic Pd/Sn Catalysts. *J. Phys. Chem. B* **1997**, *101*, 2797–2805.

(47) De Roo, J.; Ibáñez, M.; Geiregat, P.; Nedelcu, G.; Walravens, W.; Maes, J.; Martins, J. C.; Van Driessche, I.; Kovalenko, M. V.; Hens, Z. Highly Dynamic Ligand Binding and Light Absorption Coefficient of Cesium Lead Bromide Perovskite Nanocrystals. *ACS Nano* **2016**, *10*, 2071–2081.

(48) Liu, Y.; Cadavid, D.; Ibáñez, M.; De Roo, J.; Ortega, S.; Dobrozhan, O.; Kovalenko, M.; Cabot, A. Colloidal AgSbSe2nanocrystals: Surface Analysis, Electronic Doping and Processing into Thermoelectric Nanomaterials. *J. Mater. Chem. C* **2016**, *4*, 4756–4762.

(49) Mansfield, M. L.; Douglas, J. F.; Mansfield, M. L.; Douglas, J. F. Transport Properties of Rodlike Particles. *Macromolecules* **2008**, *41*, 5422–5432.

(50) Wu, Y.; Cai, S.; Wang, D.; He, W.; Li, Y. Syntheses of Water-Soluble Octahedral, Truncated Octahedral, and Cubic Pt-Ni Nanocrystals and Their Structure-Activity Study

in Model Hydrogenation Reactions. *J. Am. Chem. Soc.* **2012**, *134*, 8975–8981.

(51) Segura, Y.; López, N.; Pérez-Ramírez, J. Origin of the Superior Hydrogenation Selectivity of Gold Nanoparticles in Alkyne + Alkene Mixtures: Triple- versus Double-Bond Activation. *J. Catal.* **2007**, *247*, 383–386.

(52) Yoo, B. S.; Choi, N. S.; Shim, C. Y.; Son, Y.; Lee, S. W. Electrophilic Attack of Alkyl Halide at the Cyanide Nitrogen in Trans-[Fe(H)(CN)(dppe)$_2$]: Preparation, Structure, and Properties of Trans-[Fe(H)(CNR)(dppe)$_2$]X (Dppe = $Ph_2PCH_2CH_2PPh_2$; R = Me, Et, Pr, I-Pr, *n*-Bu, CH_2CH_2Br, $CH_2CH_2CH_2I$, $CH_2CH{=}CH_2$, $CH_2C{\equiv}CH$. *Inorganica Chim. Acta* **2000**, *309*, 137–145.

(53) Wang, H. S.; Wang, Y. C.; Pan, Y. M.; Zhao, S. L.; Chen, Z. F. Simultaneous Reduction of Nitro- to Amino-Group in the Palladium-Catalyzed Suzuki Cross-Coupling Reaction. *Tetrahedron Lett.* **2008**, *49*, 2634–2637.

TOC